PREPRINT.
Ender Özden and Ilker Tari, "Shell side CFD Analysis of a Small Shell-and-tube Heat Exchanger," Energy Conversion and Management, Vol. 51, No. 5, pp. 1004-1014 (2010).

SHELL SIDE CFD ANALYSIS OF A SMALL SHELL-AND-TUBE HEAT EXCHANGER

Authors:
Ender Ozden, Ilker Tari *
Department of Mechanical Engineering,
Middle East Technical University,
06531, Ankara, Turkey

* Corresponding Author. Tel.: +90 312 210 2551; Fax: +90 312 210 2536
e-mail: itari@metu.edu.tr

Abstract
The shell side design of a shell-and-tube heat exchanger; in particular the baffle spacing, baffle cut and shell diameter dependencies of the heat transfer coefficient and the pressure drop are investigated by numerically modeling a small heat exchanger. The flow and temperature fields inside the shell are resolved using a commercial CFD package. A set of CFD simulations is performed for a single shell and single tube pass heat exchanger with a variable number of baffles and turbulent flow. The results are observed to be sensitive to the turbulence model selection. The best turbulence model among the ones considered is determined by comparing the CFD results of heat transfer coefficient, outlet temperature and pressure drop with the Bell-Delaware method results. For two baffle cut values, the effect of the baffle spacing to shell diameter ratio on the heat exchanger performance is investigated by varying flow rate.

Keywords: CFD; heat exchangers; shell and tube; baffle spacing; turbulence models

Nomenclature

B	central baffle spacing (mm)
B_c	baffle cut (%)
$C_{1\varepsilon}$, $C_{2\varepsilon}$, $C_{3\varepsilon}$, C_μ, C_1, C_2	constants of transport equations
C_{b1}, C_{b2}, C_{w1}, C_{w2}, C_{w3}, C_{v1}	closure coefficients of transport equations
D_s	shell size (mm)
d	distance from the wall for near wall treatment (m)
d_o	tube outer diameter (mm)
f_{v1}, f_w	viscous damping function
g	gravitational acceleration (m/s^2)
G_b	generation of turbulence due to buoyancy
G_k	production of turbulence kinetic energy due to mean velocity gradients
k	kinetic energy of turbulent fluctuations per unit mass
k	thermal conductivity (W/m.K)
L	heat exchanger length (mm)
N_b	number of baffles
N_t	number of tubes
p	pressure (Pa)
q	heat flux as a source term (W/m^2)
S	scalar measure of the deformation tensor
S_ε , S_k, S_v	user defined source terms of transport equations

T	temperature (K)
u, v, w	velocity components (m/s)
$\vec{V}$	velocity vector
x, y, z	position coordinates

Greek Symbols

ε	viscous dissipation rate (m^2/s^3)
κ	closure coefficient of transport equations
λ	viscosity coefficient
μ	dynamic viscosity (Pa s)
μ_t	turbulent viscosity (Pa s)
ν	molecular viscosity (m^2/s)
ρ	density (kg/m^3)
σ_k	turbulent Prandtl numbers for k
σ_ε	turbulent Prandtl numbers for ε
σ_v	constant of transport equations
τ	shear stress (N/m^2)
Φ	dissipation function

1. Introduction

Shell-and-tube heat exchangers in various sizes are widely used in industrial operations and energy conversion systems. Tubular Exchanger Manufacturers Association (TEMA) regularly publishes standards and design recommendations (9th edition is published in 2007 [1]). Shell-and-tube heat exchangers have been very successfully designed according to TEMA standards and using recommended correlation based analytical approaches. These approaches have constantly improved since the early days due to accumulating industrial experience and operational data, and improving instrumentation. The correlation based approaches can be used for sizing and can also be used iteratively to obtain general performance parameters (rating) of a heat exchanger. At a given iteration, if the performance of the considered design is calculated to be unsatisfactory, a better performing design can be obtained by changing the design parameters in the right direction. An experienced heat exchanger designer knows what to change in which direction. As the simplest example: if the tube side heat transfer coefficient comes out smaller than expected, one can guess that the velocities are low and try a configuration with a smaller cross-sectional flow area in the next iteration. Although it is relatively simple to adjust the tube side parameters, it is very hard to get the right combination for the shell side. If possible, an ability to visualize the flow and temperature fields on the shell side can simplify the assessment of the weaknesses, thus directs the designer to the right direction. Computational Fluid Dynamics (CFD) can be very useful to gain that ability.

The shell side flow is very complicated in shell-and-tube heat exchangers due to many different leakage paths and bypass streams between different flow zones. For different shell designs and sizes, the importance of each one of the leakage and bypass streams may vary. However in small heat exchangers, these streams either do not exist or are negligible compared to the main flow stream. The heat exchanger model used in this study is comparatively small sized; therefore compared to the main stream, all of the leakage and bypass streams can be neglected. Even for such shell geometry, the shell side flow still has a complicated structure due to the existence of baffles. Baffles are used for directing the flow inside the shell from the inlet to the outlet while maintaining effective circulation of the shell side fluid hence providing effective use of the heat transfer area. Single segmental baffle that is used in the present study is the most common baffle type. It has a cut allowing the fluid to pass through in parallel or counter flow direction. The baffle cut (B_c) is measured as a percent of the baffle diameter. A number of baffles are placed along the shell in alternating orientations (cut facing up, cut facing down, cut facing up again, etc.) in order to create flow paths across the tube bundle (forming cross flow windows). The spacing between baffles (B) determines the structure of the stream. In the configuration shown in Figure 1, equally spaced six baffles are used. Flow and heat transfer characteristics are very sensitive to baffle spacing and baffle cut. The importance of baffle cut and baffle spacing is schematically shown in Figure 2. For a given shell geometry, the ideal configuration depends on both the baffle cut and the baffle spacing. When these values are smaller than ideal, the main stream passing the cut window is reflected by the next baffle and unwanted recirculation zones form. When they are larger than ideal, the main stream follows a path near the next baffle and again recirculation zones form behind the baffle. Heat transfer area corresponding to recirculation zones

can not be used effectively. In the present study, effects of baffle spacing on the heat transfer and the pressure drop are analyzed by considering two different baffle cut values.

The most commonly used correlation based approaches for designing the shell side are the Kern method [2] and the Bell-Delaware method [3]. The Kern method gives conservative results and is only suitable for the preliminary sizing. The Bell-Delaware method is a very detailed method and is usually very accurate in estimating the shell side heat transfer coefficient and the pressure drop for common shell side geometric arrangements. When the Bell-Delaware method is used for rating, it can indicate the existence of possible weaknesses in the shell side design, but it can not pin point where these weaknesses are.

To be able to understand the causes of the shell side design weaknesses, the flow phenomenon inside the shell must be well understood. For that purpose, numerous analytical, experimental and numerical studies have been performed. Most of these studies were concentrated on the certain aspects of the shell-and-tube heat exchanger design. Among others, Gay et al. [4] worked on heat transfer, while Halle et al. [5], Pekdemir et al [6], Gaddis and Gnielinski [7] investigated pressure drop. Some of the researchers concentrated only on certain parts of the shell-and-tube heat exchanger. Li and Kottke [8], [9] and Karno and Ajib [10] investigated the effect of tube arrangement on the heat transfer. Sparrow and Reifschneider [11], Eryener [12], Karno and Ajib [13] studied the effects of baffle spacing on both the heat transfer and the pressure drop. As a result of these studies, baffle cut and baffle spacing are identified as the most important geometric parameters effecting both pressure drop and heat transfer characteristics on the shell side. In the present study, we concentrate on these two parameters by eliminating aforementioned leakage and bypass streams in our shell-and-tube heat exchanger design that is modeled for detailed Computational Fluid Dynamics (CFD) simulations.

Compared to correlation based methods, the use of CFD in heat exchanger design is very limited. CFD can be used both in the rating, and iteratively in the sizing of heat exchangers. It can be particularly useful in the initial design steps, reducing the number of testing of prototypes and providing a good insight in the transport phenomena occurring in the heat exchangers [14]. To be able to run a successful full CFD simulation for a detailed heat exchanger model, large amounts of computing power and computer memory as well as long computation times are required. Without any simplification, an industrial shell-and tube heat exchanger with 500 tubes and 10 baffles would require at least 150 million computational elements, to resolve the geometry [15]. It is not possible to model such geometry by using an ordinary computer. To overcome that difficulty, in the previous works, large scale shell-and-tube heat exchangers are modeled by using some simplifications. The commonly used simplifications are the porous medium model and the distributed resistance approach. Prithiviraj and Andrews [15], [16] modeled shell-and-tube heat exchangers using distributed resistance approach. By using this method, a single computational cell may have multiple tubes; therefore, shell side of the heat exchanger was modeled by relatively coarse grid. Sha et al. [17] developed a multidimensional, thermal-hydraulic model in which shell side was modeled using surface permeability, volumetric porosity and distributed resistance approaches. He et al. [18] modeled three types of

shell-and-tube heat exchangers using a distributed resistance approach with a modified porous medium model. Stevanovic et al. [19] performed numerical analysis of three dimensional fluid flow and heat transfer in a shell-and-tube heat exchanger in which the baffles and the tube bundle were modeled using porous media. In all of these simplified approaches, the shell side pressure drop and heat transfer rate results showed good agreement with experimental data.

With these simplified approaches, one can predict the shell side heat transfer coefficient and pressure drop successfully, however for visualization of the shell side flow and temperature fields in detail, a full CFD model of the shell side is needed. With ever increasing computational capabilities, the number of elements or cells that can be used in a CFD model is increasing. For double-pipe heat exchangers, there are two recent studies using full CFD models [20][21], however to our knowledge there is none for shell-and-tube heat exchangers. Today, it is also possible to model a small shell-and-tube heat exchanger in detail with the available computers and software. By modeling the geometry as accurately as possible, the flow structure and the temperature distribution inside the shell can be obtained. This detailed data can be used for calculating global parameters such as heat transfer coefficient and pressure drop that can be compared with the correlation based ones. Furthermore, the data can also be used for visualizing the flow and temperature fields which can help to locate the weaknesses in the design such as recirculation and relaminarization zones. The objective of the present study is to explore the possibilities and limitations of full CFD modeling and analysis of the shell side by using current desktop computer technology and a current commercial CFD software, thus filling the gap in the literature.

In this study, a small shell-and-tube heat exchanger is modeled for CFD simulations. A commercial CFD package, ANSYS Fluent version 6.3 [22], is used together with Gambit mesh generation software. Sensitivity of the simulation results to modeling choices such as mesh and turbulence model is investigated. After selecting a suitable mesh, a discretization scheme and a turbulence model, simulations are performed for three different shell side flow rates by varying baffle spacing and baffle cut. The simulation results are used for calculating shell side heat transfer coefficient and pressure drop. These results are compared with the Kern and the Bell-Delaware results.

2. Modelling Details

In this study, a small heat exchanger is selected in order to increase the model detail and to make solid observations about the flow inside the shell. Some of the design parameters and the predetermined geometric parameters are presented in Table 1. The geometric model with six baffles is shown in Figure 1. Two different baffle cut values are selected: 25% baffle cut value is very common in shell-and-tube heat exchanger designs; whereas, 36% baffle cut value is selected to place the cut just below or above the central row of tubes. The working fluid of the shell side is water. Since the properties of water are defined as constants in the Fluent database, to improve the accuracy, they are redefined using piecewise-linear functions of temperature by using the “Thermo-Physical Properties of Saturated Water” tables available in the literature [23].

2.1 Governing equations

The governing equations of the flow are modified according to the conditions of the simulated case. Since the problem is assumed to be steady, time dependent parameters are dropped from the equations. The resulting equations are:

Conservation of mass: $$\nabla.(\rho \vec{V}) = 0 \quad (1)$$

x-momentum: $$\nabla.(\rho u \vec{V}) = -\frac{\partial p}{\partial x} + \frac{\partial \tau_{xx}}{\partial x} + \frac{\partial \tau_{yx}}{\partial y} + \frac{\partial \tau_{zx}}{\partial z} \quad (2)$$

y-momentum: $$\nabla.(\rho v \vec{V}) = -\frac{\partial p}{\partial y} + \frac{\partial \tau_{xy}}{\partial x} + \frac{\partial \tau_{yy}}{\partial y} + \frac{\partial \tau_{zy}}{\partial z} + \rho g \quad (3)$$

z-momentum: $$\nabla.(\rho w \vec{V}) = -\frac{\partial p}{\partial z} + \frac{\partial \tau_{xz}}{\partial x} + \frac{\partial \tau_{yz}}{\partial y} + \frac{\partial \tau_{zz}}{\partial z} \quad (4)$$

Energy: $$\nabla.(\rho e \vec{V}) = -p\nabla.\vec{V} + \nabla.(k\nabla T) + \dot{q} + \Phi \quad (5)$$

In Eq. (5), Φ is the dissipation function that can be calculated from

$$\Phi = \mu \left[\begin{array}{l} 2\left[\left(\frac{\partial u}{\partial x}\right)^2 + \left(\frac{\partial v}{\partial y}\right)^2 + \left(\frac{\partial w}{\partial z}\right)^2 \right] + \\ \left(\frac{\partial u}{\partial y} + \frac{\partial v}{\partial x}\right)^2 + \left(\frac{\partial u}{\partial z} + \frac{\partial w}{\partial x}\right)^2 + \left(\frac{\partial v}{\partial z} + \frac{\partial w}{\partial y}\right)^2 \end{array} \right] + \lambda \left(\nabla.\vec{V}\right)^2 \quad (6)$$

2.2. Boundary conditions

The desired mass flow rate and temperature values are assigned to the inlet nozzle of the heat exchanger. The shell inlet temperature is set to 300 K. Zero gauge pressure is assigned to the outlet nozzle, in order to obtain the relative pressure drop between inlet and outlet. The inlet velocity profile is assumed to be uniform. No slip condition is assigned to all surfaces. The zero heat flux boundary condition is assigned to the shell outer wall, assuming the shell is perfectly insulated outside.

Since the tube side flow is easy to resolve, the present study is concentrated on the shell side flow. After modeling the tubes as solid cylinders, the constant wall temperature of 450 K is assigned to the tube walls.

2.3. Mesh selection

Mesh generation is performed using Gambit. The surfaces of the model are meshed using quadrilateral elements. The shell volume is meshed using tetragonal-hybrid elements. Two different mesh sizes are used in the six baffle case: the coarse mesh with approximately 700,000 elements; and a finer mesh with approximately 1,360,000 elements.

2.4. Turbulence model

Since the flow in this study is turbulent, turbulence effects should be taken into account using turbulence modeling. The choice of turbulence model is very critical in CFD simulations [24]. However, there is no universal criterion for selecting a turbulence model. The turbulence model used in one study may not work in a different study. It is advisable to try a few different turbulence models.

In this study, the Spalart-Allmaras [25] and two different k-ε turbulence models are tried. In the Spalart-Allmaras turbulence model, only one turbulence equation is solved, therefore it is the least expensive model in ANSYS Fluent considering the computational effort. Two types of k-ε turbulence model are tried: standard and realizable. The transport equations, the viscosity calculation method, and the constants used in the model are the main differences between these models [22].

The Spalart-Allmaras model is a one-equation model that solves a modeled transport equation for the turbulent viscosity. This model includes eight closure coefficients and three closure functions. For steady state, the model equations are as follows [26];

$$\frac{\partial}{\partial x_i}(\rho \tilde{\nu} u_i) = \rho \tilde{\nu} C_{b1} \tilde{S} - C_{w1} f_w \rho \left(\frac{\tilde{\nu}}{d}\right)^2 + \frac{1}{\sigma_{\tilde{\nu}}}\left[\frac{\partial}{\partial x_j}\left\{(\nu + \mu)\frac{\partial \tilde{\nu}}{\partial x_j}\right\} + C_{b2}\rho\left(\frac{\partial \tilde{\nu}}{\partial x_j}\right)^2\right] + S_{\tilde{\nu}} \tag{7}$$

$$\mu_t = \rho f_{v1} \tilde{\nu} \tag{8}$$

Equation (7) is the transport equation and Equation (8) is the turbulent viscosity equation. In Equation (7), i or j = 1, 2, 3 represents the three components of the variables in x, y and z direction. And the closure coefficients are given as follows:

$$C_{w1} = \frac{C_{b1}}{\kappa^2} + \frac{(1 + C_{b2})}{\sigma_{\tilde{\nu}}} \tag{9}$$

$C_{b1} = 0.1355$ $\quad C_{b2} = 0.622$ $\quad C_{v1} = 7.1$ $\quad \sigma_{\tilde{\nu}} = 2/3$

$C_{w2} = 0.3$ $\quad C_{w3} = 2.0$ $\quad \kappa = 0.4187$

The standard k-ε model is a semi-empirical model based on model transport equations for the turbulence kinetic energy k and its dissipation rate ε. For steady state, k and ε are obtained from the following transport equations:

$$\frac{\partial}{\partial x_i}(\rho k u_i) = \frac{\partial}{\partial x_j}\left[(\mu + \frac{\mu_t}{\sigma_k})\frac{\partial k}{\partial x_j}\right] + G_k + G_b - \rho\varepsilon + S_k \tag{10}$$

$$\frac{\partial}{\partial x_i}(\rho \varepsilon u_i) = \frac{\partial}{\partial x_j}\left[(\mu + \frac{\mu_t}{\sigma_\varepsilon})\frac{\partial \varepsilon}{\partial x_j}\right] + C_{1\varepsilon}\frac{\varepsilon}{k}(G_k + C_{3\varepsilon}G_b) - C_{2\varepsilon}\rho\frac{\varepsilon^2}{k} + S_\varepsilon \tag{11}$$

And the turbulent viscosity is defined by the following equation:

$$\mu_t = \rho C_\mu \frac{k^2}{\varepsilon} \tag{12}$$

The model constants have the following values:

$C_{1\varepsilon} = 1.44$ $\quad C_{2\varepsilon} = 1.92$ $\quad C_\mu = 0.09$ $\quad \sigma_k = 1.0$ $\quad \sigma_\varepsilon = 1.3$

The main differences between the realizable k-ε model and the standard k-ε model are; a new formulation for the turbulent viscosity included in the realizable model, and for the dissipation rate ε different transport equation is derived. In realizable k-ε model, for steady state, ε is obtained from the following transport equation:

$$\frac{\partial}{\partial x_j}(\rho\varepsilon u_j) = \frac{\partial}{\partial x_j}\left[(\mu + \frac{\mu_t}{\sigma_\varepsilon})\frac{\partial \varepsilon}{\partial x_j}\right] + \rho C_1 S\varepsilon + C_{1\varepsilon}\frac{\varepsilon}{k}C_{3\varepsilon}G_b - C_2\rho\frac{\varepsilon^2}{k+\sqrt{\varepsilon\nu}} + S_\varepsilon \quad (13)$$

The model constants have the following values:

$C_{1\varepsilon} = 1.44 \quad C_2 = 1.9 \quad \sigma_k = 1.0 \quad \sigma_\varepsilon = 1.2$

2.5. Other modeling choices

The first order and second order discretization schemes are tried in the analysis. In the first order discretization, the standard scheme is selected for pressure, and the first order upwind scheme is selected for momentum, turbulent kinetic energy and dissipation rate. In the second order discretization, the standard second order scheme is selected for pressure, and the second order upwind scheme is selected for momentum, turbulent kinetic energy and dissipation rate.

On one hand, the first order discretization usually has a better convergence than the second order. On the other hand, it generally gives less accurate results. Discretization errors are reduced in higher order schemes, since more neighboring points are included [27].

The convergence criterion is taken as 10^{-6} for the pressure residual, and 10^{-3} for all of the other residuals.

3. Results and discussion

For verification of our general CFD modeling approach, in a previous study [28], the accuracy of a full CFD model for a laminar flow heat exchanger was demonstrated by comparing the results with the available experimental data from a very small educational demonstration unit with two baffles. As the first step of the present study, for a larger heat exchanger with turbulent flow, the sensitivity of the results to the turbulence model and to the discretization order is investigated for three different shell side mass flow rate values (§3.1). Then, with the selected turbulence model and discretization scheme, variations of the shell side heat transfer coefficient and pressure drop values with the flow rate and the baffle spacing are investigated (§3.2). Finally, the effects of baffle cut on the heat transfer and the pressure drop are investigated (§3.3).

3.1 Sensitivity of results to turbulence model and discretization order

In all of the preliminary simulations, the flow inside the shell is observed to be turbulent. Therefore, the viscous model is selected as turbulent. The sensitivity of the results to the turbulence model and the discretization order is investigated using the heat exchanger model with six baffles which is shown in Figure 1. The first and second order discretization schemes, and three different turbulence models are tried for two different mesh densities. The results of the analyses are presented in Table 2.

CFD results are presented on the left side of the table. The shell side outlet temperature, shell side pressure drop and total heat transfer rate values are obtained directly from the CFD runs. The heat transfer coefficient values are calculated using the log-mean-temperature-difference (LMTD) method [23] from the temperature difference and the heat transfer area. In LMTD, for the shell side outlet temperature, the CFD simulation results are used.

The correlation based approaches; the Kern method [2] and the Bell-Delaware method [3] are used in the analytical calculations. In the pressure drop calculations, the work of Kapale and Chand [29] is used.

It is observed that the Kern Method under predicts the heat transfer coefficient in all cases. Since Kern method is a conservative approach, that result is expected. The Bell-Delaware method shows a better agreement with the CFD results in the overall heat transfer coefficient calculation. In general, the difference increases by increasing the mass flow rate. For the selection of the modeling parameters, CFD results are compared with the Bell-Delaware results for each combination of parameters (cases in Table 2). After eliminating the cases leading to unexpected results, the case showing the best agreement with the Bell-Delaware is selected for modeling.

Cases B, D and D-2 are the ones eliminated first, because in these cases, unexpectedly, the shell side outlet temperature increases with the increasing mass flow rate and the total heat transfer rate results are not acceptable. In cases A, E and E-2, k-ε standard turbulence model is used. Since the behavior of the shell side outlet temperature differs in these cases, and the deviation of the total heat transfer rate from the Bell-Delaware result increases with the decreasing mass flow rate, they are also eliminated. In the remaining cases: C, F and F-2, k-ε realizable turbulence model is used. For these cases, the behavior of the shell side temperature difference is as expected. That is, the shell side outlet temperature decreases by increasing the mass flow rate. Also, the difference between the total heat transfer rate values is reasonable. Among them, Case F gives the best agreement and the parameters corresponding to this case: k-ε realizable turbulence model, the first order discretization and fine mesh are selected for the modeling.

For all of the cases in Table 2, the pressure drop is lower in the analytical calculations. The main reason for that is the selected baffle spacing to shell diameter ratio B/D_s=0.96 which is selected for being within the recommended region suggested by [30] as indicated in Figure 3, for B_c=36%. The pressure drop is strongly affected by the baffle spacing. The analytical methods under predict the pressure drop, if the window flow area is considerably less than the cross flow area [31]. Contrary to [30], Mukherjee [32] suggested that, the optimum B/D_s ratio should be between 0.3 and 0.6. Our observations also agree with that suggestion, and B/D_s should be reduced to improve the pressure drop results. Therefore, in the following section, increased N_b values are considered for a fixed heat exchanger length.

3.2 Effect of baffle spacing on pressure drop and heat transfer

The effects of the baffle spacing on the heat transfer and the pressure drop are investigated for four different numbers of baffles (N_b) with 36% baffle cut. The

corresponding central baffle spacing and B/D_s ratio values are presented in Table 3. After adjusting the baffle spacing or N_b, the model is re-meshed using the previous mesh parameters of the finer mesh in §3.1. The k-ε realizable turbulence model is used in this part with the first order discretization scheme. The number of elements for the 12 baffle case is increased to 1,568,850.

The percent differences between the analytical and the CFD analysis results by taking the analytical ones as the reference are presented in Table 4. The corresponding data set for 6, 8, 10 and 12 baffles are given in Table 5. By decreasing the baffle spacing (increasing N_b), the agreement of the results is improved, as expected. In the overall heat transfer calculation, percent difference with the Kern method shows no improvement.

For 8, 10 and 12 baffles, the percent difference results with respect to the Bell-Delaware method are improved. For 0.5 kg/s and 1 kg/s mass flow rates, the percent difference decreased below 10%, by adjusting B/D_s ratio. But, for 2 kg/s the percent difference is still high. The pressure drop results of the CFD analyses are also improved. In the 12 baffle case, the difference is reduced below 10%. There is also an improvement in the total heat transfer rate prediction. The percent difference is reduced below 2%, for the 10 and 12 baffle cases.

In Figures 4-7, velocity path lines for 6, 8, 10 and 12 baffles are given for the shell side mass flow rate of 1 kg/s. In Figures 4 and 5 that are respectively for 6 and 8 baffles, it is observed that the flow hits the baffle plate, and the direction of the flow is changed. Therefore, the shell space behind the baffle is not effectively used for cross-flow, as marked with a circle in Figure 4. Recirculation zones appear in these regions, as indicated with a circle in Figure 5. In Figures 6 and 7 that are for 10 and 12 baffles, the flow is observed to be well developed. The cross flow paths are established throughout the shell volume and the recirculation zones disappear. That explains the more accurate results obtained for 10 and 12 baffles in Table 4. Considering that the Bell-Delaware method was based on a very large collection of data from operational heat exchangers (accepted designs), it is expected that only an acceptable shell side design gives matching CFD results.

3.3 Effects of baffle cut on pressure drop and heat transfer

Here, the simulations are repeated for the baffle cut value of 25% and effects of the baffle cut on the heat transfer and the pressure drop are investigated. The calculation procedure is the same as the previous section. Similar to the previous sections, the shell side outlet temperature, the shell side pressure drop and the total heat transfer rate values are obtained directly from the CFD runs. The percent differences between the analytical calculations and the CFD analysis results are presented in Table 6. The analytical calculations are taken as the base values for the percent difference calculations.

By comparing the results in Table 6 with the ones in Table 4, the agreement with the Kern method results is better for 25% baffle cut case, due to the fact that Kern method assumes B_c=25%. The agreement still can be considered acceptable only for 0.5 kg/s mass flow rate.

When Bell-Delaware results are taken as the reference values, it is observed that for all N_b values, the agreements in heat transfer coefficient and pressure drop are better in case of B_c=25%. That can be attributed to the fact that 25% baffle cut is the most common baffle cut, thus the large part of the Bell-Delaware data is obtained from heat exchangers with 25% baffle cut. Therefore, it should be expected for Bell-Delaware to give more accurate results at that baffle cut. Although it is hard to compare both B_c results, because the percent differences are in single digits or even below 1%, in general, the agreement is slightly better for B_c=25%.

Particle velocity path lines for 0.5 kg/s flow rate are presented in Figure 8 indicate the locations of the main stream flows. In the sub-figures, the parts of the shell without any or with a few particle paths correspond to recirculation zones in which the heat transfer area is not utilized effectively. When the percent differences with the Bell-Delaware results in Tables 4 and 6 examined together with Figure 8, it is observed that N_b=10 and B_c=25% combination gives the smallest difference in both heat transfer coefficient and pressure drop results and also shows very well covered cross flow window in Figure 8. Agreement in N_b=12 and B_c=25% case is comparatively worse, probably due to the reflections from the next baffle as visualized in Figure 8. For B_c=36%, N_b=12 gives the best results both according to differences in Table 4 values and the visual appearance of the flow in Figure 8.

4. Conclusion

The shell side of a small shell-and-tube heat exchanger is modeled with sufficient detail to resolve the flow and temperature fields. From the CFD simulation results, for fixed tube wall and shell inlet temperatures, shell side heat transfer coefficient, pressure drop and heat transfer rate values are obtained. The sensitivity of the shell side flow and temperature distributions to the mesh density, the order of discretization and the turbulence modeling is observed. Three turbulence models are tried for the first and the second order discretizations using two different mesh densities. By comparing with Bell-Delaware results, the k-ε realizable turbulence model with the first order discretization and the fine mesh is selected as the best simulation approach.

By varying the baffle spacing between 6 and 12, and the baffle cut values of 36% and 25%, for 0.5, 1 and 2 kg/s shell side flow rates, the simulation results are compared with the results from the Kern and Bell-Delaware methods. It is observed that the Kern method always under predicts the heat transfer coefficient. For properly spaced baffles, it is observed that the CFD simulation results are in very good agreement with the Bell-Delaware results. The results are also sensitive to the baffle cut selection, for this heat exchanger geometry 25% baffle cut gives slightly better results. It is surprising that the differences between Bell-Delaware and CFD predictions of the total heat transfer rate are below 2% for most of the cases. That confirms the well deserved trust that Bell-Delaware method gained in the heat exchanger industry and shows the power of CFD technique as a heat exchanger design tool.

It is also observed that Figure 3 that was suggested in [30] and used as a guideline in many previous design studies contradicts with the suggestions of Mukherjee [32]. Our

numerical results and visualizations agree with [32] indicating that Figure 3 from [30] may not be appropriate to use in baffle spacing of no phase change heat exchangers.

The flow structures that are visualized using the CFD simulations showed that for the smaller number of baffles, the cross flow windows are not well utilized and some recirculation regions form behind the baffles. By increasing the number of baffles, this weakness is fixed and the heat transfer characteristics of the heat exchanger are improved. As a general conclusion, it can be said that correlation based approaches may indicate the existence of a weakness in design, but CFD simulations can also pin point the source and the location of the weakness. Using CFD, together with supporting experiments, may speed up the shell-and-tube heat exchanger design process and may improve the quality of the final design. In the near future, improvements in the computer technology will make full CFD simulations of much larger shell-and-tube heat exchangers possible.

References

[1] Standards of the Tubular Exchanger Manufacturers Association. 9th ed. Gaddis D, Ed. Tarrytown, N.Y.: TEMA Inc.; 2007.
[2] Kern DQ. Process heat transfer. New York, N.Y.: McGraw-Hill; 1950.
[3] Bell KJ. Delaware method for shell side design, in heat exchangers: thermal-hydraulic fundamentals and design. (Eds) Kakaç S, Bergles AE, Mayinger F. New York: Hemisphere; 1981;581-618.
[4] Gay B, Mackley NV, Jenkins JD. Shell-side heat transfer in baffled cylindrical shell- and-tube exchangers - an electrochemical mass transfer modelling technique. Int J Heat Mass Tran 1976;19:995-1002.
[5] Halle H, Chenoweth JM, Wabsganss MW. Shell side water flow pressure drop distribution measurements in an industrial-sized test heat exchanger. J Heat Trans 1988;110:60-7.
[6] Pekdemir T, Davies TW, Haseler LE, Diaper AD. Pressure drop measurements on the shell side of a cylindrical shell-and-tube heat exchanger. Heat Transfer Eng 1994;15:42-56.
[7] Gaddis ES, Gnielinski V. Pressure drop on the shell side of shell-and-tube heat exchangers with segmental baffles. Chem Eng Process 1997;36:149-59.
[8] Li HD, Kottke V. Visualization and determination of local heat transfer coefficients in shell-and-tube heat exchangers for staggered tube arrangement by mass transfer measurements. Exp Therm Fluid Sci 1998;17:210-6.
[9] Li HD, Kottke V. Visualization and determination of local heat transfer coefficients in shell-and-tube heat exchangers for in-line tube arrangement by mass transfer measurements. Heat Mass Transfer 1998;33:371-6.
[10] Karno A, Ajib S. Effect of tube pitch on heat transfer in shell-and-tube heat exchangers - new simulation software. Heat Mass Transfer 2006;42:263-70.
[11] Sparrow EM, Reifschneider LG. Effect of interbaffle spacing on heat transfer and pressure drop in a shell-and-tube heat exchanger. Int J Heat Mass Tran 1986;29:1617-28.
[12] Eryener D. Thermoeconomic optimization of baffle spacing for shell and tube heat exchangers. Energ Convers Manage 2006;47:1478–89.
[13] Karno A, Ajib S. Effects of baffle cut and number of baffles on pressure drop and heat transfer in shell-and-tube heat exchangers - numerical simulation. Int J Heat Exchangers 2006;7:299-322.

[14] Sunden B. Computational heat transfer in heat exchangers. Heat Transfer Eng 2007;28:895-7.
[15] Prithiviraj M, Andrews MJ. Three dimensional numerical simulation of shell-and-tube heat exchangers. Part 1: foundation and fluid mechanics. Numer Heat Transfer. Part A, Applications 1998;33:799-816.
[16] Prithiviraj M, Andrews MJ. Three dimensional numerical simulation of shell-and-tube heat exchangers. Part 2: heat transfer. Numer Heat Transfer. Part A, Applications 1998;33:817-28.
[17] Sha WT, Yang CI, Kao TT, Cho SM. Multidimensional numerical modeling of heat exchangers. J Heat Trans 1982;104:417-25.
[18] He YL, Tao WQ, Deng B, Li X, Wu Y. Numerical simulation and experimental study of flow and heat transfer characteristics of shell side fluid in shell-and-tube heat exchangers. Proc Fifth Int Conf on Enhanced, Compact and Ultra-Compact Heat Exchangers: Science, Engineering and Technology. Hoboken, NJ. Sep. 2005:29-42.
[19] Stevanović Z, Ilić G, Radojković N, Vukić M, Stefanović V, Vučković G. Design of shell and tube heat exchangers by using CFD technique – Part one: thermo hydraulic calculation. Facta Universitatis Series: Mechanical Engineering 2001;8:1091-105.
[20] Moawed MA, Ibrahim E, Gomaa A. Thermal performance of a pipe in pipe heat exchanger with sinusoidal inner pipe. Energ Convers Manage 2008;49:678–86.
[21] Chen W-L, Dung W-C. Numerical study on heat transfer characteristics of double tube heat exchangers with alternating horizontal or vertical oval cross section pipes as inner tubes. Energ Convers Manage 2008;49:1574–83.
[22] ANSYS Fluent version 6.3. Fluent 6.3 User's Guide. ANSYS Inc.
[23] Incropera FP, Dewitt DP. Fundamentals of heat and mass transfer. 4th ed. New York: J. Wiley; 1996.
[24] Sunden B. Computational fluid dynamics in research and design of heat exchangers. Heat Transfer Eng 2007;28:898-910.
[25] Spalart PR, Allmaras SR. A One-Equation turbulence model for aerodynamic flows. AIAA Paper 92-0439.
[26] Wilcox DC. Turbulence Modeling for CFD. 2nd ed. California: DCW Industries Inc; 1998.
[27] Versteeg HK, Malalasekera W. An introduction to computational fluid dynamics: the finite volume method. 1st ed. Essex, England: Pearson; 1995.
[28] Ozden E. Detailed design of shell-and-tube heat exchangers using CFD, M.S. thesis, Middle East Technical University, Ankara, Turkey, 2007.
[29] Kapale UC, Chand S. Modeling for shell-side pressure drop for liquid flow in shell-and-tube heat exchanger. Int J Heat Mass Tran 2006;49:601-10.
[30] Taborek J. Thermal and hydraulic design of heat exchangers. In: Heat Exchangers Design Handbook. Vol 3. (eds) Hewitt GF. New York: Begell House Inc; 2002.
[31] Kistler RS, Chenoweth JM. Heat exchanger shell side pressure drop: comparison of predictions with experimental data. J Heat Trans 1998;110:68-76.
[32] Mukherjee R. Effectively design shell-and-tube heat exchangers. Chem Eng Prog 1998;94:21-37.

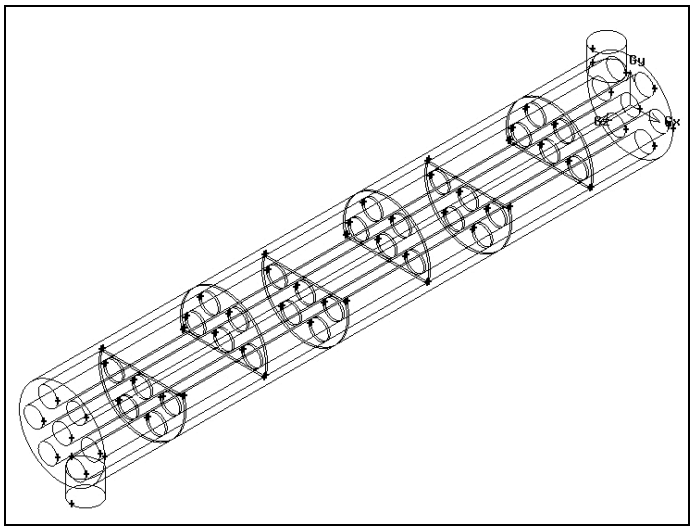

Figure 1 The model with six baffles

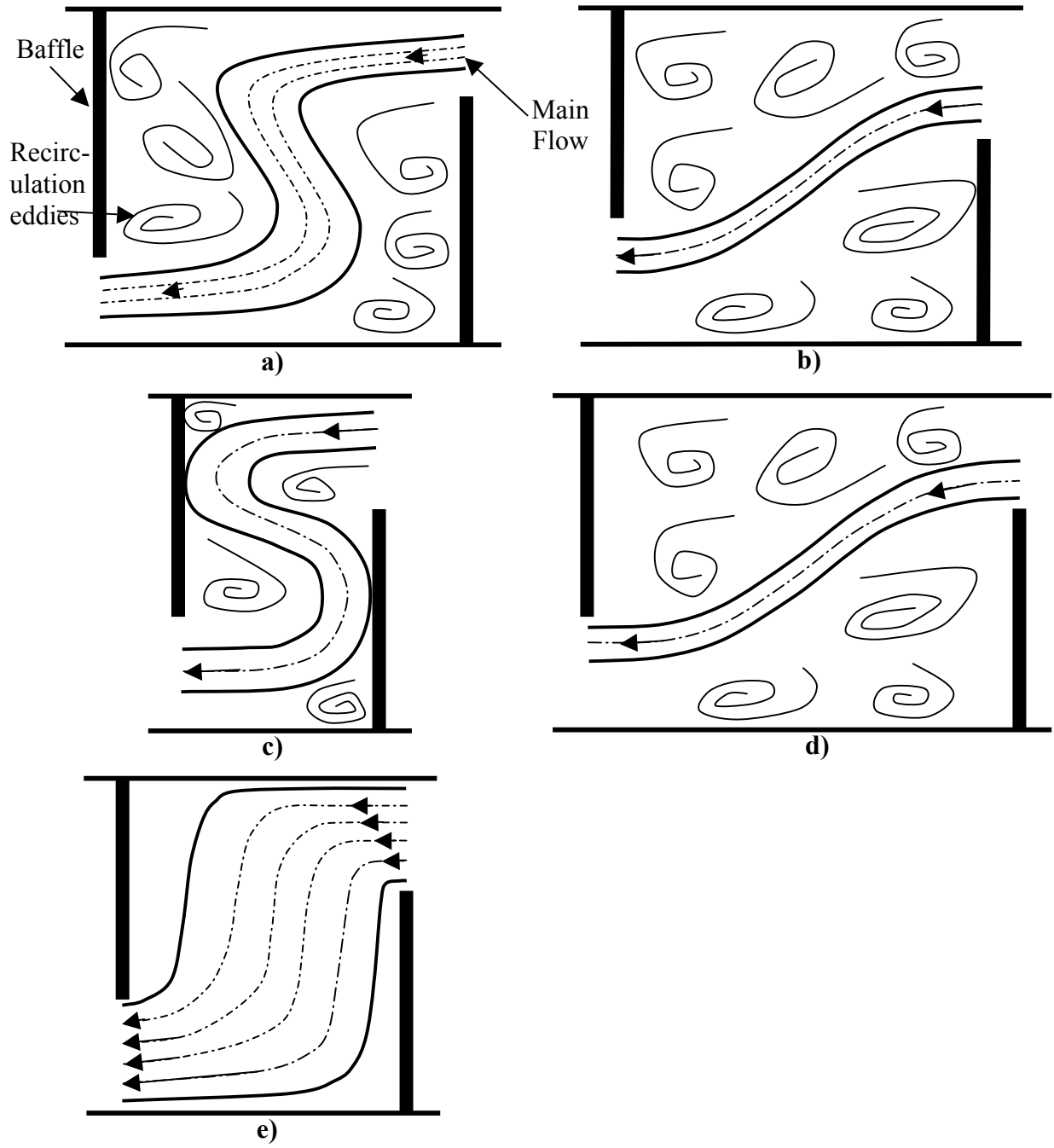

Figure 2 Effect of baffle cut and baffle spacing on the shell side main stream: a) Small baffle cut, b) Large baffle cut, c) Small baffle spacing, d) Large baffle spacing, e) Ideal baffle spacing and baffle cut

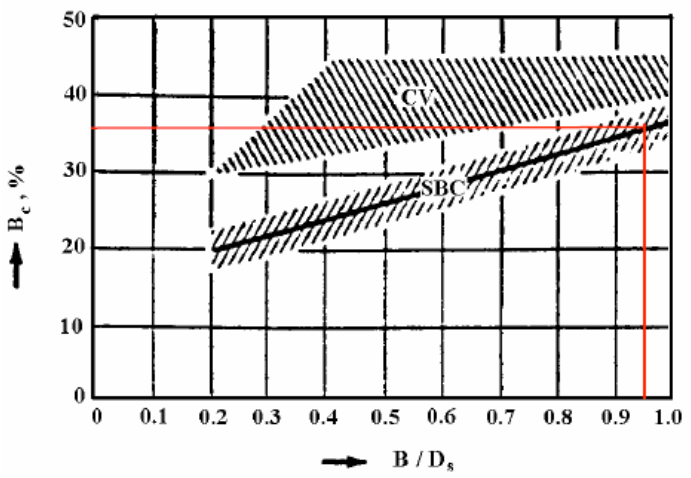

Figure 3 Bell-Delaware recommended segmental baffle cut values as a function of B/D_s ratio. SBC: segmental baffle cuts in no-phase-change flow; CV: baffle cuts applicable to condensing vapors [30].

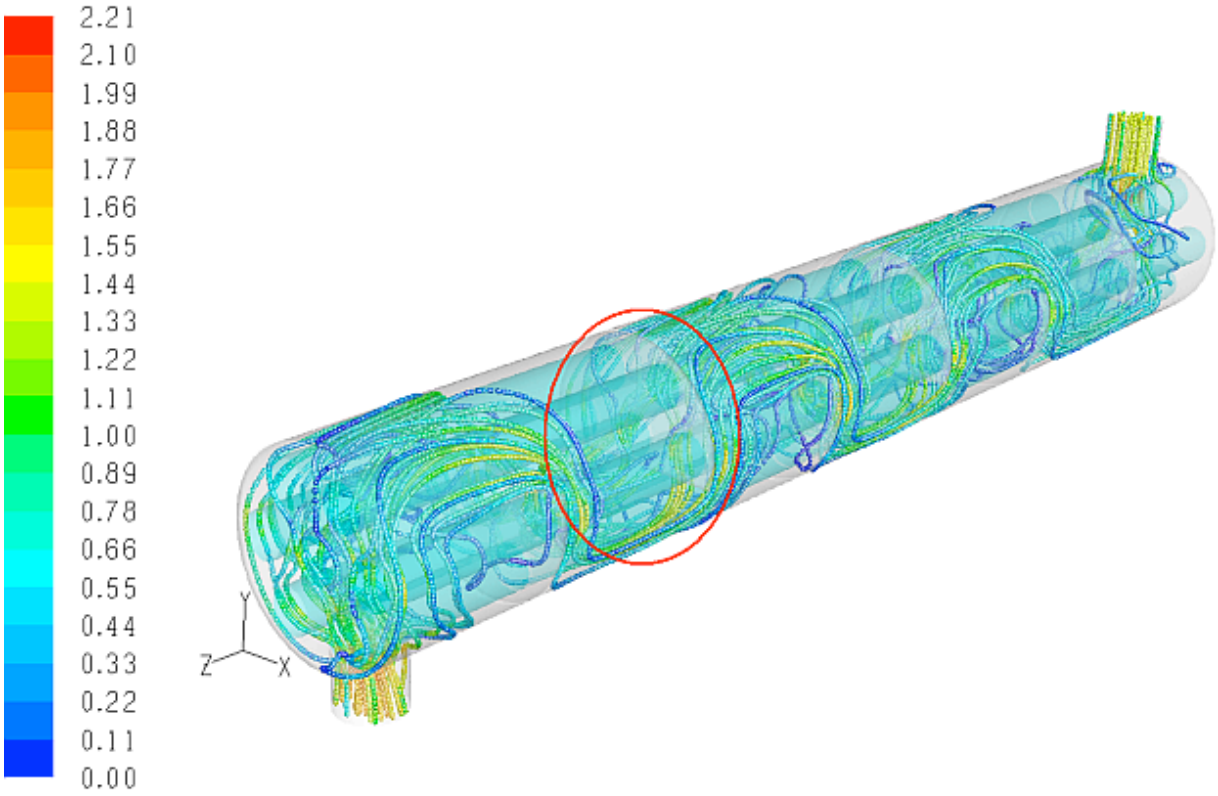

Figure 4 Velocity (m/s) path lines for 6 baffles (1 kg/s mass flow rate)

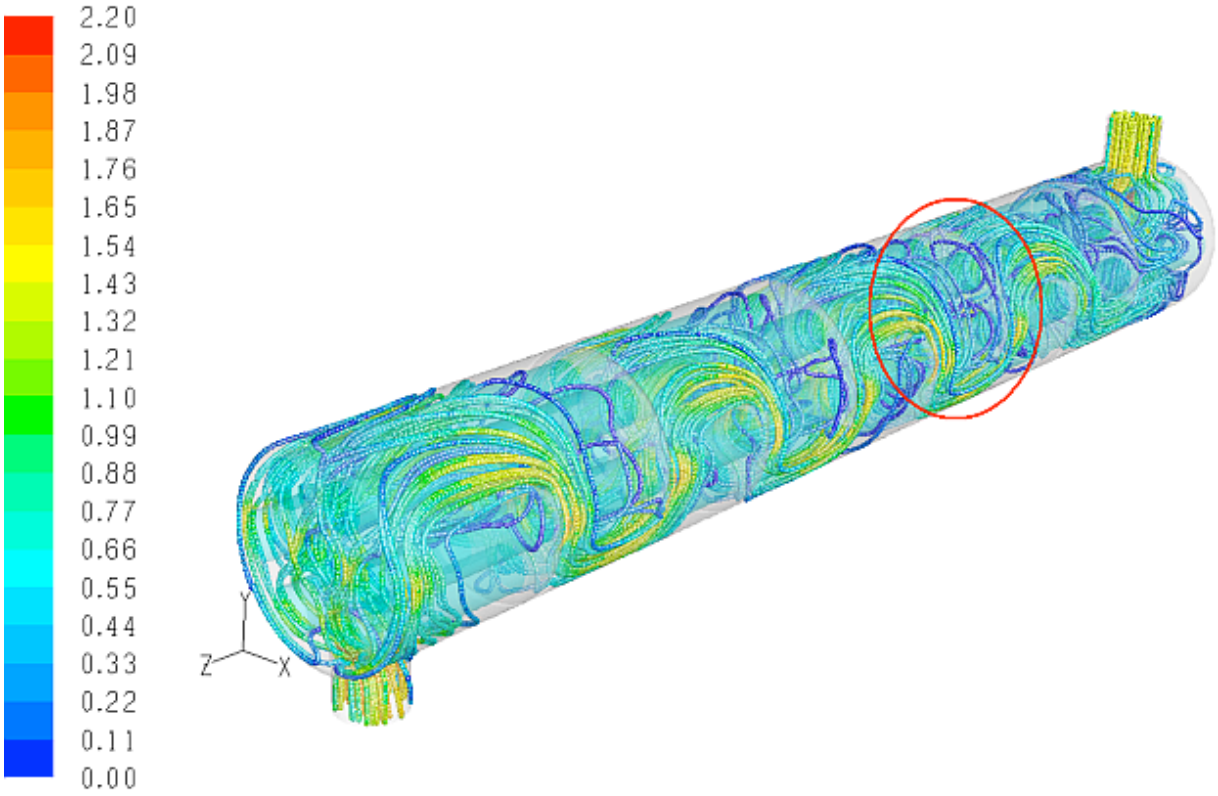

Figure 5 Velocity (m/s) path lines for 8 baffles (1 kg/s mass flow rate)

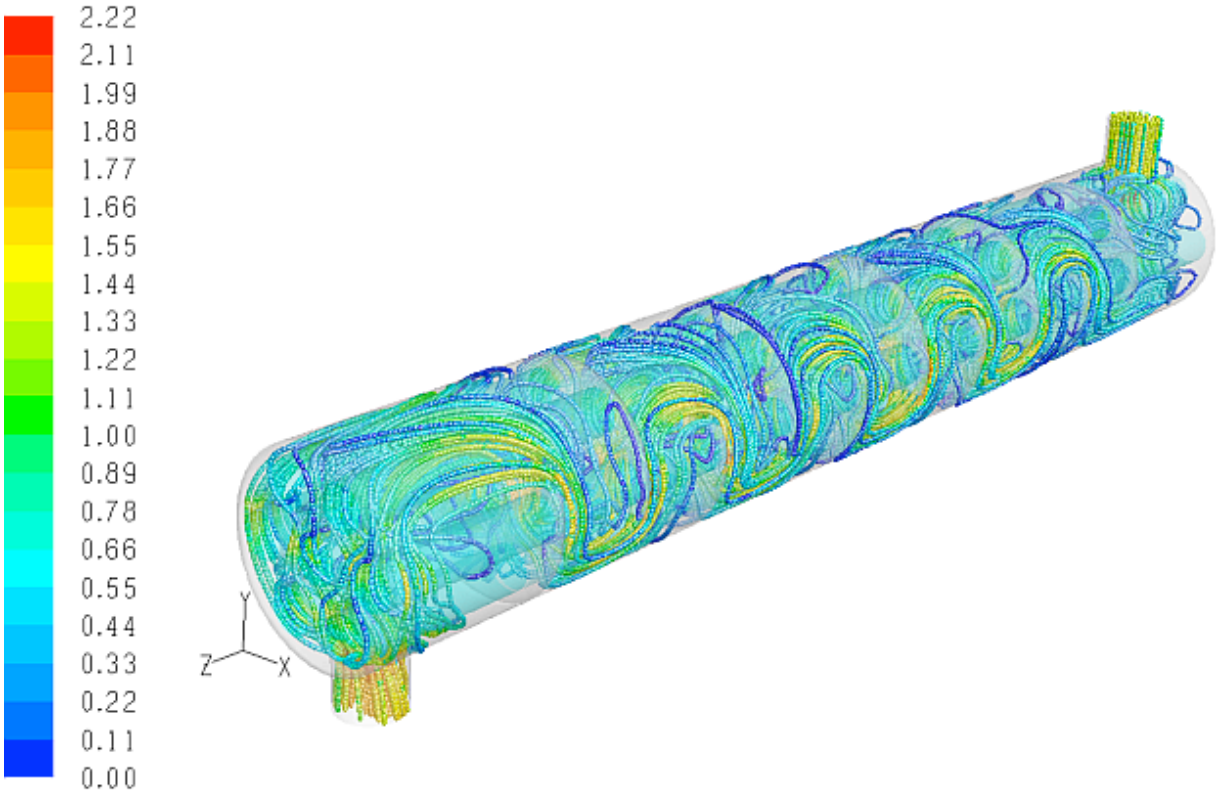

Figure 6 Velocity (m/s) path lines for 10 baffles (1 kg/s mass flow rate)

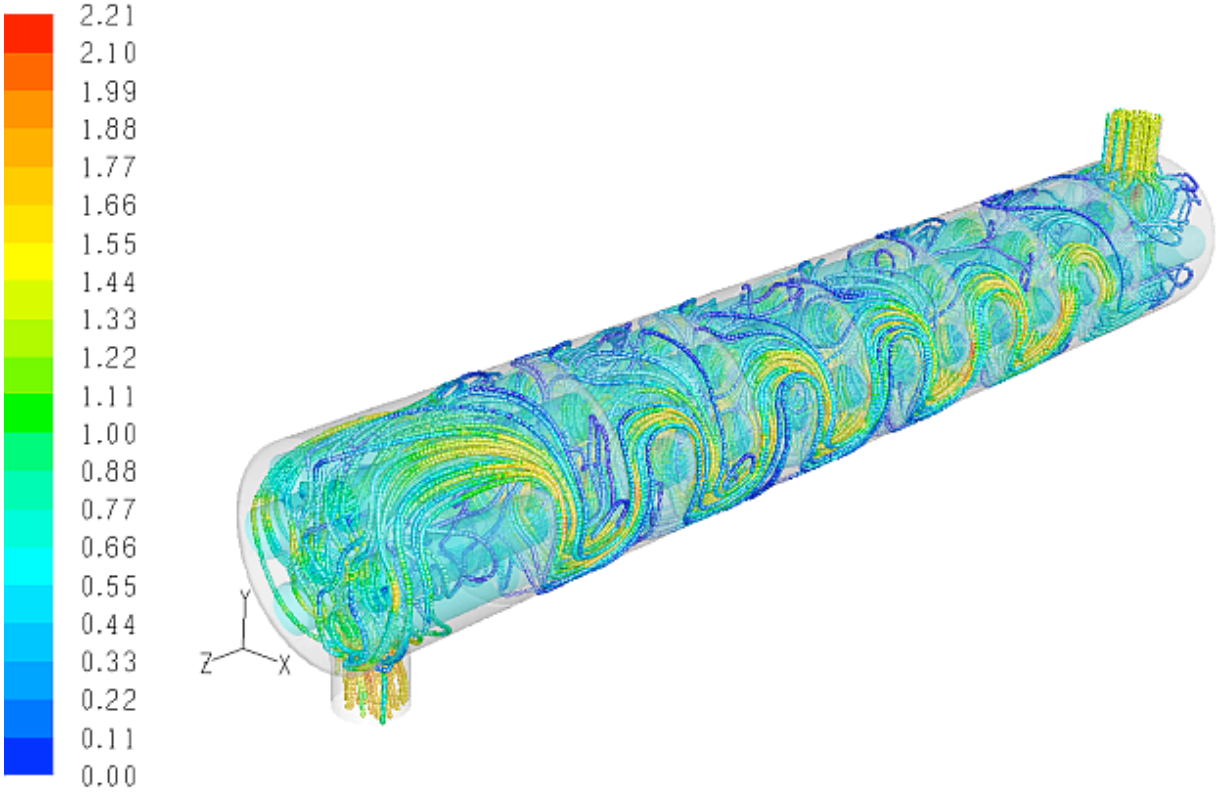

Figure 7 Velocity (m/s) path lines for 12 baffles (1 kg/s mass flow rate)

Ender Özden and Ilker Tari, "Shell side CFD Analysis of a Small Shell-and-tube Heat Exchanger," Energy Conversion and Management, Vol. 51, No. 5, pp. 1004-1014 (2010).

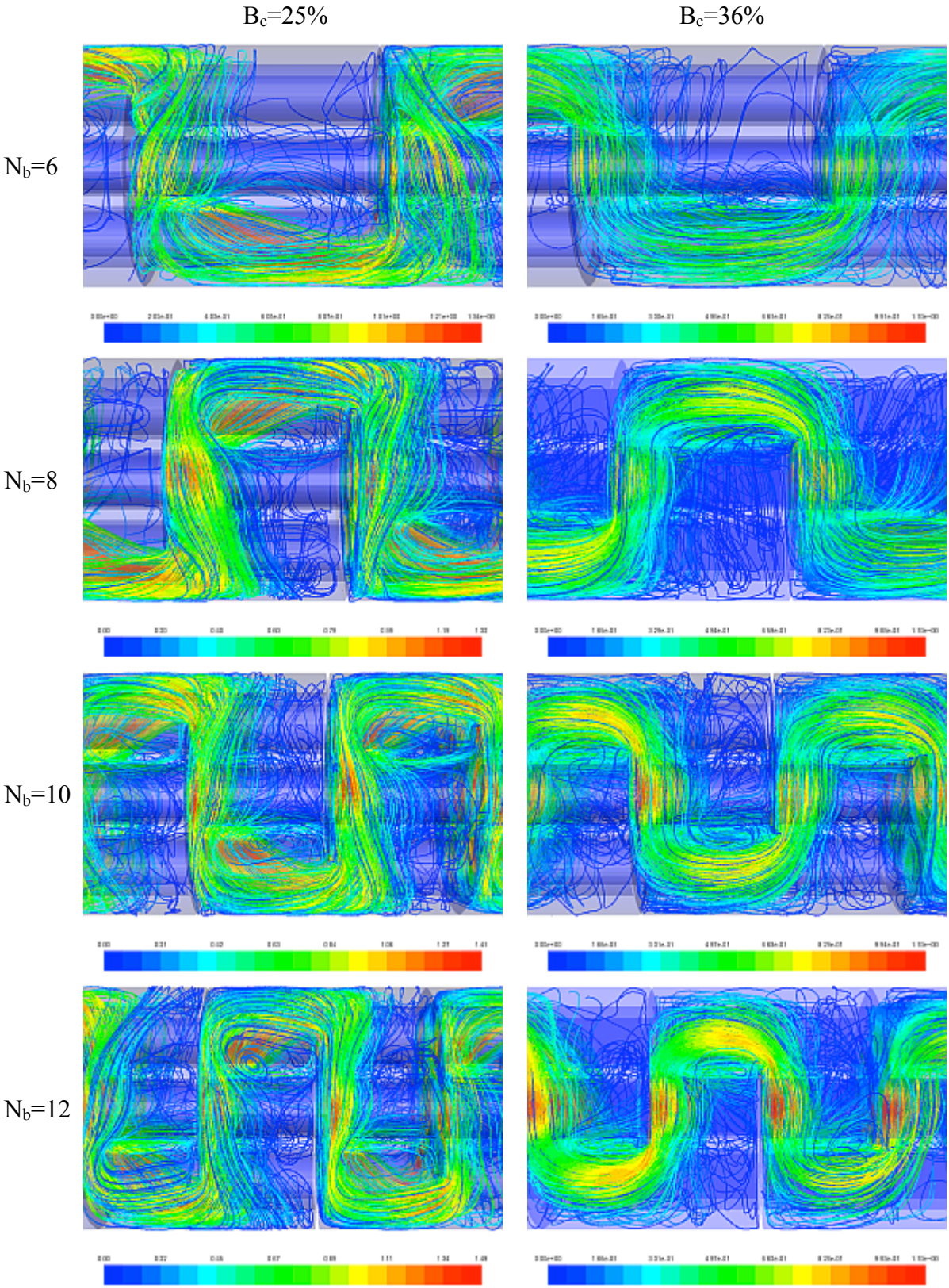

Figure 8 Particle velocity path lines for 0.5 kg/s mass flow rate. Left column is for B_c=25% and right column is for B_c=36%. Rows from top to bottom are for N_b=6, 8, 10 and 12.

Table 1 Design parameters and fixed geometric parameters

Shell size, D_s	90 mm
Tube outer diameter, d_o	20 mm
Tube bundle geometry and pitch	Triangular, 30 mm
Number of tubes, N_t	7
Heat exchanger length, L	600 mm
Shell side inlet temperature, T	300 K
Baffle cut, B_c	36 %
Central baffle spacing, B	86 mm
Number of baffles, N_b	6

Table 2 Results of the CFD analysis for different turbulence models and discretization order for N_b=6

			Results of the CFD Analysis					Analytical Calculations			
								Kern Method	Bell-Delaware Method		
Case	**Viscous Model**	**Mesh**	**Mass Flow Rate (kg/s)**	**Shell Side Outlet Temp. (K)**	**Heat Transfer Coeff. (W/m²K)**	**Shell Side Pressure Drop (Pa)**	**Total Heat Transfer Rate (W)**	**Heat Transfer Coeff. (W/m²K)**	**Heat Transfer Coeff. (W/m²K)**	**Shell Side Pressure Drop (Pa)**	**Total Heat Transfer Rate (W)**
A	*k-ε* standard	coarse mesh	0.5	321.76	2127	2153	76950	2076	2113	1230	45460
			1	326.05	3561	6648	126824	3063	3276	4587	108855
			2	327.22	6452	24692	228780	4494	5037	18650	227494
B	*k-ε* standard 2nd order	coarse mesh	0.5	320.58	2116	2209	76872	2072	2122	1234	42993
			1	325.15	3547	6732	126742	3058	3267	4585	105092
			2	326.90	6438	24792	228564	4491	5029	18640	224818
C	*k-ε* realizable	coarse mesh	0.5	334.20	2078	1509	71808	2123	2177	1242	71471
			1	327.72	3348	6112	118515	3072	3290	4592	115838
			2	325.74	6163	24464	219733	4482	5019	18630	215118
D	Spalart Allmaras	fine mesh	0.5	323.44	2323	2036	83512	2082	2121	1232	48971
			1	326.29	3654	6586	130031	3064	3277	4588	109858
			2	323.89	6151	25465	220773	4467	4992	18610	199648
D-2	Spalart Allmaras 2nd order	fine mesh	0.5	318.27	2013	2367	73713	2063	2097	1227	38166
			1	320.84	3330	7419	120845	3035	3234	4575	87074
			2	321.10	5952	27291	215792	4445	4964	18580	176321
E	*k-ε* standard	fine mesh	0.5	332.14	2501	1768	87100	2115	2167	1240	67162
			1	330.00	3941	6570	138318	3085	3306	4597	125372
			2	328.65	6994	25005	246709	4506	5113	18660	239453
E-2	*k-ε* standard 2nd order	fine mesh	0.5	325.01	2511	2162	89752	2088	2129	1233	52253
			1	327.37	3904	6714	138383	3070	3287	4591	114374
			2	328.46	6980	25068	246391	4504	5024	18630	237864
F	*k-ε* realizable	fine mesh	0.5	340.40	2514	1522	84853	2147	2213	1248	84442
			1	330.18	3757	6168	131785	3086	3311	4597	126125
			2	326.64	6768	24963	240506	4489	5025	18640	222644
F-2	*k-ε* realizable	fine mesh	0.5	343.90	2819	1547	93851	2161	2231	1251	91766
			1	337.68	4695	6198	160103	3128	3370	4616	157501

2nd order	2	332.10	8585	25702	298975	4534	5094	18700	268312

Table 3 Different number of baffles, corresponding parameters and number of elements in the models

Number of baffles, N_b	6	8	10	12
Central baffle spacing, B (mm)	86	62	48	40
B/D_s ratio	0.96	0.69	0.53	0.44
Number of elements	1,361,514	1,561,201	1,555,980	1,568,850

Table 4 Percent differences between analytical calculations and CFD analysis for B_c=36%

		Heat Transfer Coeff.		Press Drop	Total Heat Transfer Rate
Number of Baffles	**Mass Flow Rate (kg/s)**	**% difference w.r.t. Kern Method**	**% difference w.r.t. Bell-Delaware**	**% difference**	**% difference**
6	0.5	17.1	13.6	22.0	0.5
	1	21.7	13.5	34.2	4.5
	2	50.8	34.7	33.9	8.0
8	0.5	4.9	4.5	11.7	3.8
	1	14.6	7.7	22.1	0.5
	2	43.9	31.5	19.7	0.5
10	0.5	3.6	2.2	16.2	0.9
	1	9.9	6.9	11.5	1.2
	2	39.8	30.2	7.3	1.0
12	0.5	1.0	7.3	5.9	1.5
	1	18.2	3.9	0.1	1.3
	2	52.3	28.2	4.5	0.9

Table 5 Results of the CFD analysis for different baffle spacing and N_b values

		Results of the CFD Analysis				Analytical Calculations			
						Kern Method	Bell-Delaware Method		
N_b	**Mass Flow Rate (kg/s)**	**Shell Side Outlet Temp. (K)**	**Heat Transfer Coeff. (W/m²K)**	**Shell Side Pressure Drop (Pa)**	**Total Heat Transfer Rate (W)**	**Heat Transfer Coeff. (W/m²K)**	**Heat Transfer Coeff. (W/m²K)**	**Shell Side Pressure Drop (Pa)**	**Total Heat Transfer Rate (W)**
6	0.5	340.4	2514	1522	84852.9	2147	2213	1248	84442
	1	330.18	3757	6168	131785	3086	3311	4597	126125
	2	326.64	6768	24963	240506	4489	5025	18640	222644
8	0.5	341.35	2699	2206	89706	2572	2584	1975	86431
	1	334.64	4268	8634	145517	3724	3961	7069	144782
	2	332.03	7811	34371	268975	5427	5941	28720	267727
10	0.5	344.63	2869	3042	94160	2976	2933	2618	93298
	1	337.72	4736	11944	159624	4311	4432	10708	157669
	2	335.38	8784	47191	298677	6285	6745	43969	295756
12	0.5	346.34	3015	3980	98289	2984	3254	3758	96878
	1	340.31	5115	15435	170693	4328	4921	15453	168509
	2	338.36	9621	60930	323457	6318	7507	63819	320694

Table 6 Percent differences between analytical calculations and CFD analysis for B_c=%25

		Heat Transfer Coeff.		Press Drop	Total Heat Transfer Rate
Number of Baffles	**Mass Flow Rate (kg/s)**	**% difference w.r.t. Kern Method**	**% difference w.r.t. Bell-Delaware**	**% difference**	**% difference**
6	0.5	13.7	9.5	18.4	0.1
	1	20.1	12.3	32.6	0.8
	2	43.6	28.3	30.8	0.8
8	0.5	5.0	4.3	7.1	0.4
	1	11.7	7.4	17.1	2.7
	2	41.7	24.3	19.0	1.9
10	0.5	5.5	5.2	3.4	1.3
	1	15.9	10.6	10.5	1.8
	2	43.0	29.2	7.2	0.7
12	0.5	1.2	9.2	3.3	1.3
	1	16.4	0.4	10.4	1.6
	2	38.5	24.5	5.1	0.9